ChemNanoMat

CHEMNANOMAT
CHEMISTRY OF NANOMATERIALS FOR ENERGY, BIOLOGY AND MORE

ACES Asian Chemical Editorial Society

RESEARCH ARTICLE OPEN ACCESS

Insecticide@Silica Nanocontainers with High Cypermethrin Load and Improved Photostability

Mark Rutschmann | Jasmin Mokinski | Claus Feldmann

Institute of Inorganic Chemistry, Karlsruhe Institute of Technology (KIT), Karlsruhe, Germany

Correspondence: Claus Feldmann (claus.feldmann@kit.edu)

Received: 8 October 2025 | **Revised:** 25 February 2026 | **Accepted:** 13 March 2026

Keywords: cypermethrin | insecticide | nanocontainer | photostability | silica

ABSTRACT

Cypermethrin (CM) is a widely used insecticide to repel and control stinging, biting and sucking-licking insects. To limit the required CM amount, to reduce application cycles, and to increase its stability, we developed CM@OS core@shell nanocontainers (OS: *n*-octylsilicate) as a novel synthesis concept and material. The CM@OS core@shell nanocontainers are synthesized via a solvent/antisolvent approach. They exhibit a mean total diameter of 34 ± 8 nm with a CM particle core of 15 ± 3 nm in diameter and an OS particle shell of 7 ± 2 nm in thickness. Due to negative surface charging (−63 ± 1 mV), the as-prepared nanocontainers are colloidally very stable as aqueous suspensions. Analytical characterization is performed by electron microscopy (SEM, TEM, STEM), electron spectroscopy (EDXS), and additional methods (DLS, zeta-potential analysis, FT-IR, TG, C/H/N/S analysis, photometry). The CM content is 10 wt-%, and CM is photochemically significantly stabilized in regard of a cleavage of the ester group as well as of the cyclopropanyl ring in comparison to free CM. Thin-films are realized, and the slow CM release exemplary shown, and promoted by the lipophilic functionality of OS.

1 | Introduction

Nanocontainers are frequently discussed as promising shuttles for drug delivery [1, 2]. Today, new drugs can be efficiently searched and identified by methods such as combinatorial chemistry or high-throughput screening [3, 4]. In recent years, emerging drug candidates show a con-current shift to higher molecular weight and lower hydrophilicity [5, 6], which hampers a transport in aqueous media and, thus, requires new concepts for delivery [7]. While such nanocontainer concepts for pharmaceutical drugs are being intensively investigated, there are only few studies on lipophilic insecticides such as cypermethrin (CM).

CM is a synthetic pyrethroid used as an insecticide in veterinary medicine, agriculture, wood protection and in consumer products for domestic purposes [8]. It is used to repel and control stinging, biting and sucking-licking insects such as ticks, pasture flies, head flies, horse flies, lice, bird mites, or fleas. As a fast-acting neurotoxin, it acts as contact poison for insects, which are paralyzed within a few minutes after exposure [9, 10]. CM also shows an insect-repellent effect, which is based on an irritation of tactile elements in the extremities [8–10]. For application, CM is either sprayed on the walls of animal stables, directly on animals or plants, or used as prepared ear tag. In particular, rubbing by animals and/or photochemical degradation require continuously repeated application of the insecticide, which increases costs and time, and which increases the exposure for surroundings and environment. In this regard, encapsulation of CM in nanocontainers could be promising to reduce the required CM amount and the number of reapplication cycles.

Nanomaterials were yet predominately used to detect or to remove CM. For instance, the detection of CM residues in water was performed with carbon-nitride-modified graphite electrodes or silver nanodendrites [11–13]. Nanosized natural products such as nanopiperine or nanocurcumin were described to induce an antitoxic effect against CM [14–17]. Finally, silica as well as iron oxide nanoparticles were applied to remove CM remains from

water [18, 19]. In contrast, nanocontainer concepts for protection and/or controlled release of CM were rarely reported until now, and the CM load of current nanocontainers concepts is usually low with ≤1% of the total nanocontainer mass [20–23]. The highest CM loads were yet reported with about 50% in microporous silica particles [2, 24] as well as with about 75% in calcium–alginate nanoparticles [25]. In both cases, the nanoparticles were prepared with diameters of 120–250 nm by advanced microemulsion techniques, which require significant amounts of surfactants. A natural compound such as alginate, moreover, can suffer from limited long-term stability due to rapid degradation in outdoor applications. Based on our experience on drug-delivery concepts [26, 27], we here suggest CM@OS core@shell nanocontainers (OS: *n*-octylsilicate) with 10.5% CM of total nanocontainer mass and with high colloidal and chemical stability. Beside the synthesis strategy and the materials characterization, we show the formation of thin-films with promising photostability exceeding pure CM.

2 | Results and Discussion

2.1 | Synthesis

CM@OS core@shell nanocontainers were prepared using a solvent/antisolvent-type synthesis (Figure 1a). Accordingly, a mixture of octyltriethoxysilane (OTES) and ethanol was used as the solvent solution for CM and as a precursor for the formation of the OS shell (OS: octylsilicate). Demineralized water was used as the antisolvent, in which CM is insoluble. After the injection of the solvent solution into the antisolvent solution, the nucleation of insoluble CM occurred immediately. OTES served as surfactant with the lipophilic octyl chains of OTES attached to the lipophilic CM particle core, and the polar siloxane groups located on the surface of the CM particle core, which, on the one hand, limits the particle growth and, on the other hand, colloidally stabilizes the CM nanoparticles against agglomeration. To stabilize the CM particle core even further and to form a silica shell around the CM particle core, the hydrolysis of OTES was promoted by increasing the temperature (70°C), slight acidification (0.2 mL 0.1 M HCl) as well as by addition of small portions of fluoride (1 mg NH_4F) serving as a flux to support the condensation of silanol groups (Figure 1b) [28]. After formation of an OS shell of certain thickness, the suspension was neutralized (0.25 mL ammonia, 25%) to increase the surface charge of the nanocontainers and their colloidal stability (Figure 1c).

The OTES concentration was chosen in regard of an optimal colloidal and chemical stabilization of the CM particle core as well in regard of a dense OS shell not being too thick. To this concern, an OTES:CM ratio of about 10:1 turned out to be optimal. Lower OTES concentrations lead to an insufficient stabilization and the formation of agglomerates. Higher OTES concentrations are possible and increase the thickness of the OS shell. For practical handling, finally, it needs to be noticed that the CM/OTES solution was diluted with ethanol to reduce its viscosity and to facilitate the injection of the solvent solution into the antisolvent solution.

After 24 h of continuous stirring at 70°C, cross-linking of OS was finished and the suspension was left to cool to room temperature. The as-prepared CM@OS core@shell nanocontainers were purified by centrifugation and concentrated to a load of 5 mg/mL CM@OS core@shell nanocontainers in water. These suspensions are colloidally stable for several months (Figure 1d). Additional stabilizers are not required.

2.2 | Characterization

Size and structure of the CM@OS core@shell nanocontainers were examined by dynamic light scattering (DLS), scanning electron microscopy (SEM), and scanning transmission electron microscopy (STEM). To this concern, the CM@OS core@shell nanocontainers exhibit a spherical morphology (Figure 2a,b). A statistical evaluation of >150 particles on SEM images resulted in a mean particle diameter of 34 ± 8 nm (Figure 2c). This is well in agreement with DLS analysis showing a mean hydrodynamic particle diameter of 36 ± 13 nm in water. STEM images confirm the size range and the spherical morphology. Moreover, the core@shell structure of the nanoparticles becomes visible with the different contrast of the particle core and the particle shell (Figure 2d). Based on an evaluation of about 50 nanoparticles on high-angle annular dark-field scanning transmission electron microscopy (HAADF–STEM) images, a mean particle-core diameter of 15 ± 3 nm and a mean particle-shell thickness of 7 ± 2 nm can be deduced. Finally, DLS also allows to determine the zeta potential at pH = 7, which is at a value of −63 ± 1 mV for the

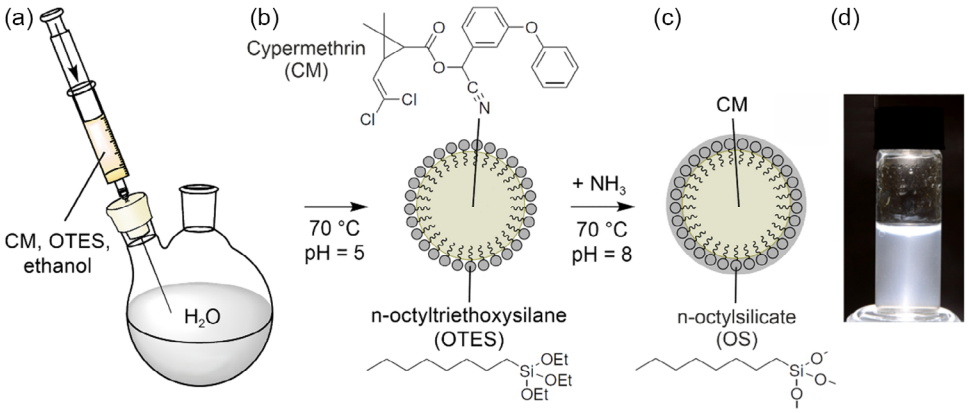

FIGURE 1 | Schematic illustration of the synthesis of CM@OS core@shell nanocontainers: (a) injection of CM/OTES/ethanol solvent into H_2O as the antisolvent; (b) stabilization of CM nanoparticles by OTES; (c) formation of OS particle shell to stabilize and encapsulate the CM particle core (CM: cypermethrin; OTES: *n*-octyltriethoxysilane; OS: *n*-octylsilicate); (d) photo of aqueous nanocontainer suspension.

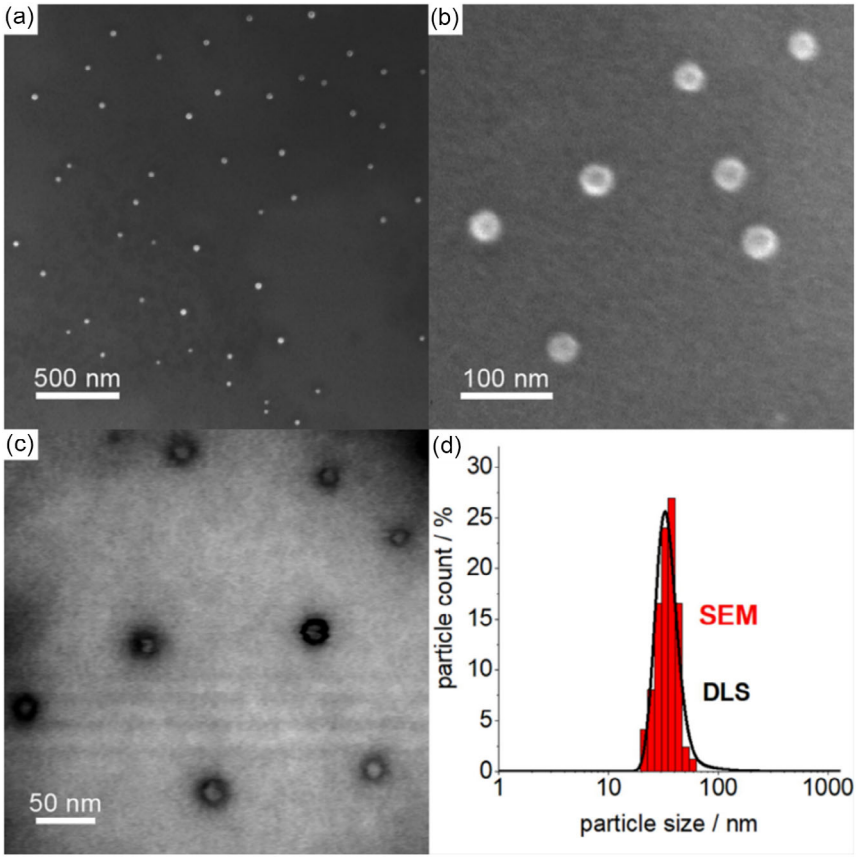

FIGURE 2 | Size, shape, and structure of the as-prepared CM@OS core@shell nanocontainers: (a) SEM overview images; (b) SEM detail image; (c) size distribution according to SEM and DLS; and (d) HAADF–STEM image.

CM@OS core@shell nanocontainers. This also explains the good colloidal stability of the as-prepared suspensions in water. In this respect, aqueous suspensions exhibiting a zeta potential above + 30 mV or below −30 mV are usually considered to be colloidally stable. The high negative charging of the CM@OS core@shell nanocontainers can be attributed to the OS shell. Silica typically shows negative surface charging in the range of −80 to −50 mV at neutral pH [29].

To verify the presence of the core@shell structure, SEM and TEM in combination with energy dispersive X-ray spectroscopy (EDXS) were used. The EDXS signals obtained with pressed pellets in a SEM device can be assigned to silicon ($K_\alpha = 1.739$ keV), chlorine ($K_\alpha = 2.621$ keV), oxygen ($K_\alpha = 0.525$ keV), and carbon ($K_\alpha = 0.277$ keV) (Figure 3a). In particular, the signal of silicon can be assigned to the OS shell. The chlorine signal originates from CM. Signals of oxygen and carbon are nonspecific. Especially for carbon, it must be noticed that the samples were prepared on adhesive carbon pads (SEM) or Lacey-carbon copper grids (TEM), so that only part of the carbon signal originates from the nanocontainers.

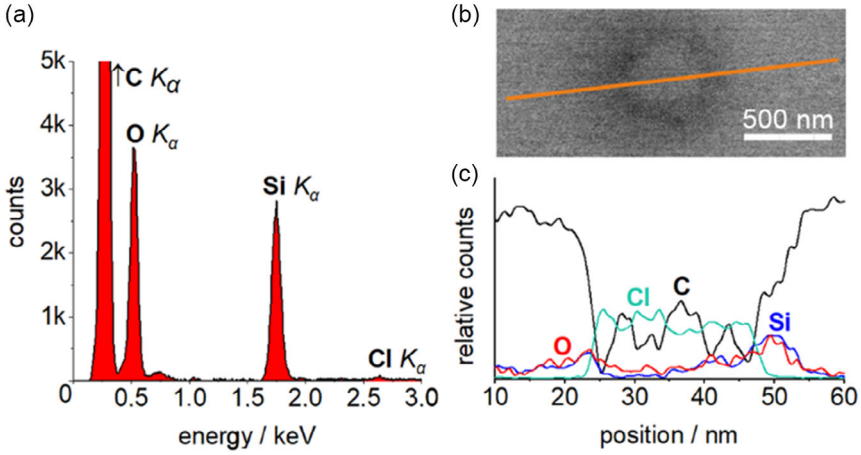

FIGURE 3 | Structure of the as-prepared CM@OS core@shell nanocontainers: (a) EDXS spectrum of a pressed pellet of the sample (EDXS-SEM); (b) HAADF–STEM image; and (c) EDXS linescan along the red line on the HAADF–STEM image in (b).

To prove the core@shell structure of the nanocontainers, EDXS linescans were performed (Figure 3b,c). Here, HAADF–STEM images already evidence the higher electron absorption of the OS shell and the lower electron absorption of the CM core (Figure 3b). The EDXS linescan shows the expected concentration profile with a high chlorine concentration in the center of the nanocontainer and the typical dip–shaped curve of the concentration profiles of silicon and oxygen (Figure 3c). The considerable increase of the carbon signal outside the nanocontainer can be attributed to the uncovered Lacey-carbon copper grid, on which the nanocontainers were deposited. Based on the EDXS linescan, a particle–core diameter of 15–25 nm and a thickness of 10 nm of the particle shell were deduced, which is in accordance with HAADF–STEM images (Figure 2d).

To examine the chemical composition and CM load of the CM@OS core@shell nanocontainers, X-ray powder diffraction (XRD), Fourier-transform infrared (FT-IR) spectroscopy, elemental analysis (EA), and photometry with UV–vis spectroscopy were performed. XRD does not show any Bragg reflections and indicates the nanocontainers to be amorphous. The broad Bragg reflection at about 5° of 2θ originates from silica and can be related to small-angle scattering. In fact, this is not a surprise as the formation of silica at low temperature usually does not result in any crystalline product (Figure 4a). Qualitatively, the presence of OS and CM was confirmed by FT-IR spectroscopy (Figure 4b). Thus, a comparison with reference spectra clearly shows (Si–O–Si) vibrations at 1500–950 and 850–450 cm^{-1} [30]. Moreover, vibrations ν(COO) of the ester group at 1737 cm^{-1}, $\nu(C_{aromat}–C_{aromat})$ at 1650 and 1587 cm^{-1}, δ(C–H) at 1487 cm^{-1} originate from CM. The fingerprint region (1450–900 cm^{-1}) is less characteristic due a superposition by the vibrations of OS. Furthermore, ν(C–H) vibrations (3000–2850 cm^{-1}) are also less significant as they may stem from CM as well as from OS.

EA allows to quantify a carbon content of 56.4 wt%, a hydrogen content of 9.1 wt%, a nitrogen content of 0.34 wt% and, in sum, a total organics content of 65.8 wt% with a remain for Si/Cl/O of 34.2 wt%. As CM is the only N-containing component, a total load of 10.1 wt% CM can be deduced for the CM@OS core@shell nanocontainers based on the EA results. With these data, moreover, the C, H, Cl, O content originating from CM can be calculated to 6.4 wt% C, 0.46 wt% H, 1.7 wt% Cl, and 1.2 wt% O. The difference between total C/H content and the C/H content originating from CM (i.e., 56.4 – 6.4 = 50.0 wt% C; 9.10–0.46 = 8.64 wt% H) allows to extract the OS content (OS: $C_8H_{17}O_{3/2}Si$, octylsilicate, after hydrolyzation of the three ethoxy groups) to about 86 wt-% with a C:H ratio (5.8) that also fits well with the expected ratio of OS (5.6). Furthermore, a Si:Cl ratio of 25:1 was determined by EDXS (i.e., 17.8 wt% Si, 0.7 wt% Cl), which is well in accordance with contents of about 90 wt% OS and 10 wt% CM of the CM@OS core@shell nanocontainers. Specifically, the CM content is again in good agreement with the CM content obtained by EA.

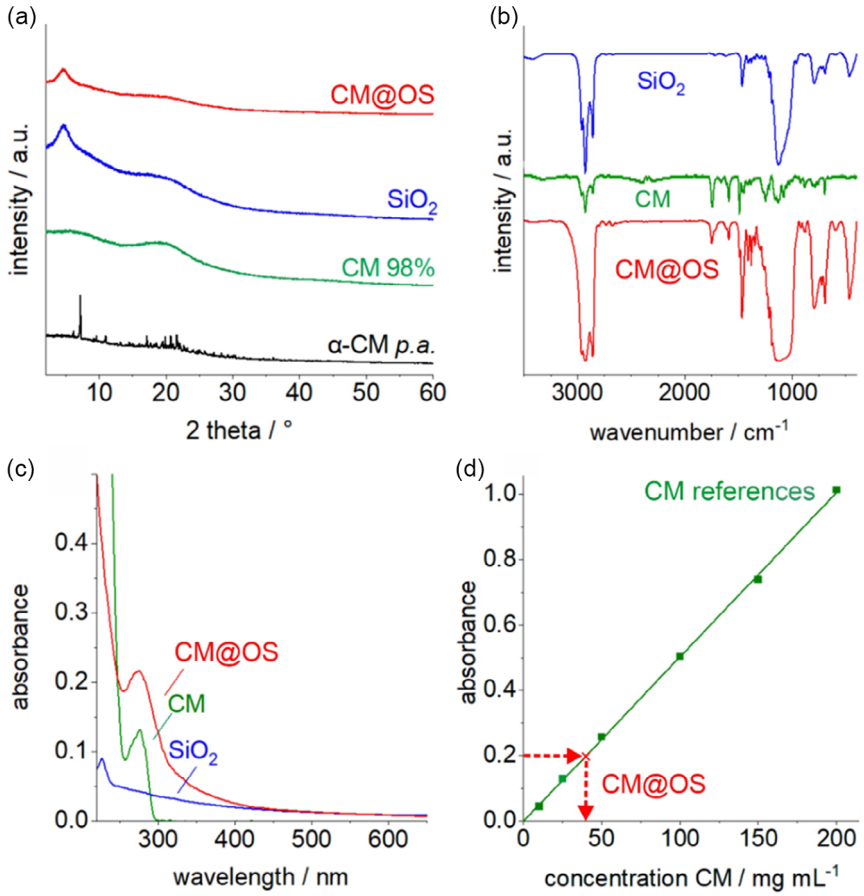

FIGURE 4 | Composition of the as-prepared CM@OS nanocontainers: (a) XRD; (b) FT-IR spectra; and (c) UV–vis spectra. All with nonfilled OS hollow spheres and pure CM as references. (d) Photometric determination of CM-load in the nanocontainers (red, dispersed in water) based on calibration curve with CM references (green; CM concentrations: 10, 25, 50, 100, 150, and 200 µg/mL, all dissolved in ethanol).

Finally, the CM concentration was determined by photometry, which is possible since CM exhibits an absorption maximum in the UV at 276 nm (Figure 4c). To this concern, several reference solutions with different CM concentrations were prepared (i.e., 10, 25, 50, 100, 150, and 200 µg/mL). Here, it needs to be noticed that these solutions were prepared in ethanol as CM is almost insoluble in water. The photometric analysis resulted in a suitable calibration curve with linear regression (Figure 4d). Based on this calibration, the CM content of the CM@OS core@shell nanocontainers was determined to 10.5%. This amount is in good agreement with the values obtained by EA and EDXS and validates the composition of the nanocontainers and their CM load even further.

2.3 | Photostability and Thin-Films

In addition to the chemical composition and nanostructure, we have investigated the photostability of the CM@OS nanocontainers in comparison to free CM. The photostability is relevant for the practical application of insecticides (e.g., in animal stables) as a photochemical degradation makes it necessary to reapply the insecticide, which, on the one hand, increases time and costs and, on the other hand, multiplies the total amount of insecticide used. Within the class of the pyrethroid-type insecticides, CM is generally known for comparably high photostability in daylight with a half-life ranging from 17 to 110 days [31]. However, a photodegradation of 45% was reported within 2 days for solutions in methanol when exposed to UV light with wavelengths below 290 nm. Particularly shorter wavelengths in the UV cause an accelerated photodegradation with, for instance, a decomposition of 90% after 3 days on glass substrates [32].

To evaluate the photostability of CM in CM@OS nanocontainers, time-resolved UV–Vis spectroscopy and FT-IR spectroscopy were used. Surprisingly, kinetic analyses over 24 h with UV-vis spectroscopy using the absorption at 276 nm with continuous UV irradiation at 220 nm shows an increased absorption of + 0.04% for the CM@OS nanocontainers and an even higher increase of absorption of +4.67% for free CM (Figure 5a). With the expectation of a UV-initiated photochemical degradation, such increase of absorption was unexpected but can be explained by the specific chemistry of the CM molecule (Figure 5b). According to the literature, CM is photochemically most sensitive to a cleavage of the ester group (Figure 5b: indicated by arrow 1) and a cleavage of the cyclopropanyl ring (Figure 5b: indicated by arrow 2) [33, 34]. From these two options, the formation of 3-phenoxybenzoic acid after cleavage of the ester group would retain the molecules π-system. In contrast, a photochemical cleavage of the cyclopropanyl ring results in a new conjugated double bond and an extension of the π-system [35], which accounts for the observed optical absorption. Thus, the increased absorption after 24 h points to a proceeding photochemical cleavage of the cyclopropanyl ring. The fact that this increase in absorption is lower for CM in CM@OS nanocontainers as for free CM indicates a protective effect of the OS shell, which protects and stabilizes CM in the particle core of the nanocontainers.

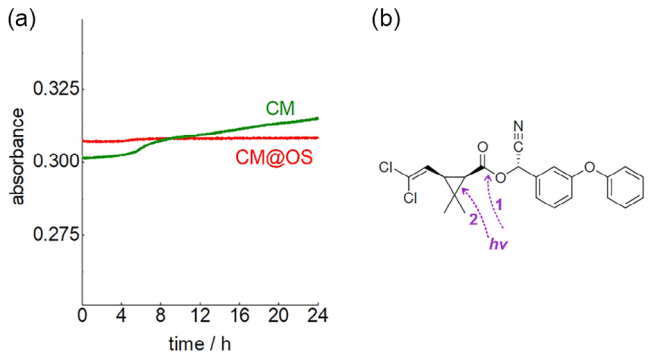

FIGURE 5 | Photostability of CM@OS nanocontainer suspensions (red) in comparison to free CM (green): (a) Time-resolved UV–Vis spectra over 24 h while tracking the absorbance at 276 nm with irradiation at 220 nm and (b) optional mechanisms for photochemical degradation of CM with cleavage of the ester group (indicated by arrow1) or cleavage of the cyclopropanyl ring (indicated by arrow 2) [33–35].

To validate the effect of a photochemical ester cleavage and/or a ring-opening of the cyclopropanyl functionality, the absorption intensity related in the C = O vibration at 1660 cm^{-1} and the vibration of the cyclopropanyl ring at 881 cm^{-1} [36] were monitored by FT-IR spectroscopy prior to UV irradiation as well as 2 and 4 h after UV exposure (at 254 nm) (Figure 6a,d). Here, a significant increase of the absorption intensity of the C = O vibration as well as a significant decrease of the intensity of the cyclopropanyl-related vibration were observed for free CM (Figure 6c,f), which, again, indicates photochemical ring opening and, thus, degradation of CM. In contrast, the spectra of the CM@OS nanocontainers show only minor variation of both the absorption intensities of the C = O vibration and the cyclopropanyl-related vibration (Figure 6b,e). In sum, both UV–Vis and FT-IR spectroscopy show CM to be predominately unaffected under UV irradiation when encapsulated in CM@OS nanocontainers. Thus, the OS shell allows to protect CM from photochemical degradation. For comparison and evaluation, it needs to be considered that free CM was dissolved in ethanol (due to its insolubility in water), whereas the CM@OS nanocontainers were dispersed in water. The number of OH radicals formed under UV irradiation, however, is significantly higher in water than in ethanol [37]. In sum, CM in CM@OS nanocontainers are not only more stable than free CM, even more the conditions for the CM@OS nanocontainers were also harsher than for free CM, which further points to the stabilizing effect for CM upon encapsulation in CM@OS nanocontainers.

In regard of an application-oriented scenario, the CM release and the suitability of the CM@OS nanocontainers for thin-film coatings were evaluated (Figures 7 and 8). The CM release was exemplarily tested with CM@OS core@shell nanocontainers suspended in water, ethanol (EtOH) and tetrahydrofuran (THF). These three solvents mimic different scenarios of hydrophilic and lipophilic conditions with water being most hydrophilic and THF being most lipophilic. From the application point-of-view, CM should be released only slowly into water (rain, condensed water) but needs to be released to the lipophilic extremities of insects. As pure silica is highly hydrophilic itself, we used OS with the octyl functionality to support a slow diffusion of lipophilic CM from the inside of the nanocontainers to the nanocontainer surface. To this concern, suspensions of CM@OS core@shell nanocontainers were stirred for 12 h in the respective solvent. Thereafter, the nanocontainers were separated by centrifugation, and the presence of CM in the supernatant was analyzed via UV–Vis spectroscopy (Figure 7a). As a result, almost no CM was released into water (Figure 7b). Ethanol and THF show CM release, which is about 10-times

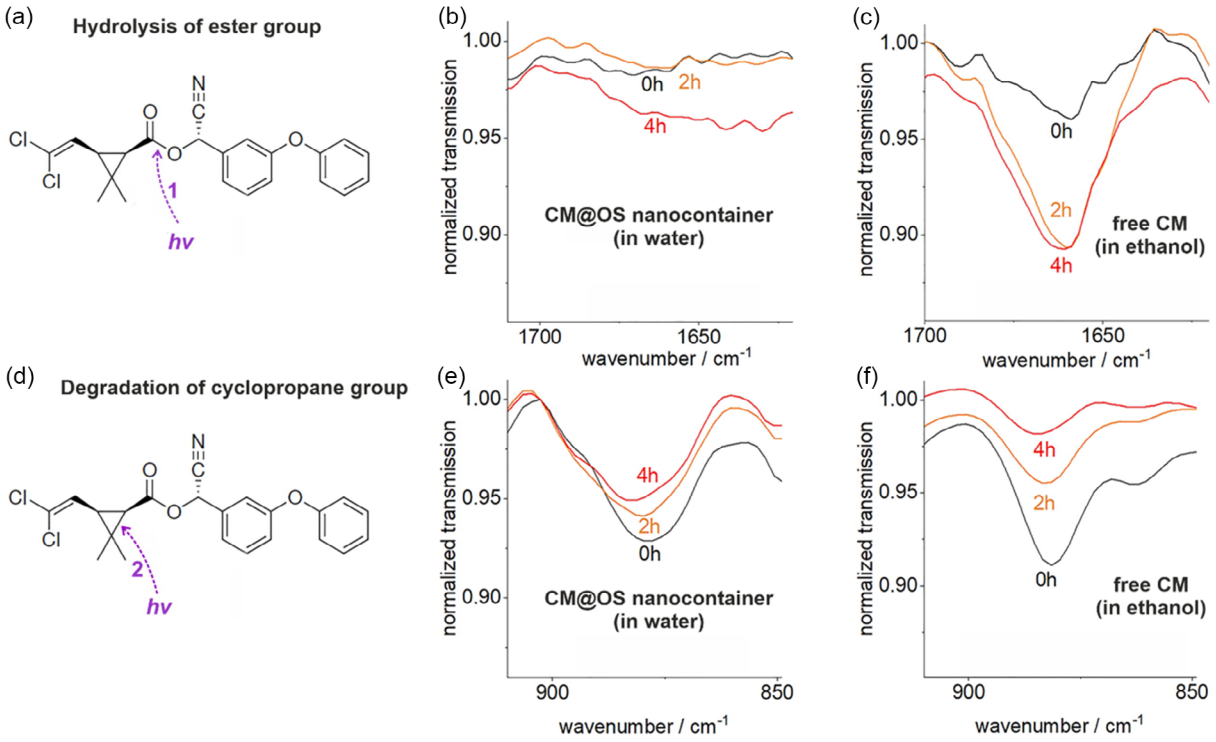

FIGURE 6 | Photostability of CM@OS nanocontainers (suspension in water) in comparison to free CM (in ethanol) over 2 and 4 h of UV irradiation (254 nm): (a) Scheme of photochemical cleavage of the ester group; (b,c) FT-IR spectra showing the absorption intensity of the C=O vibration (1660 cm^{-1}) for the nanocontainers (b) and free CM (c); (d) scheme of photochemical cleavage of the cyclopropanyl ring; and (e,f) FT-IR spectra showing the absorption intensity of the cyclopropanyl-related vibration (881 cm^{-1}) for the nanocontainers (e) and free CM (f).

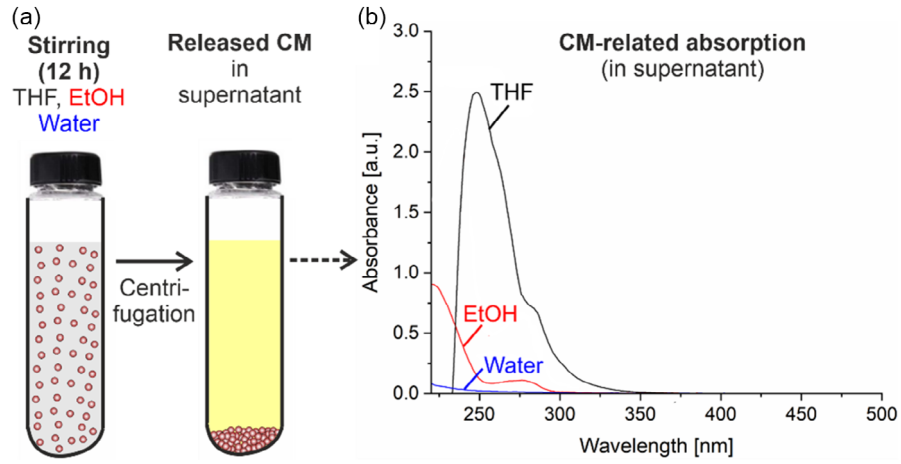

FIGURE 7 | Release of CM in water, ethanol, and THF after 12 h of stirring in suspension: (a) Scheme illustrating the stirring of suspensions with released CM analyzed after centrifugation in the supernatant and (b) absorption of CM at 276 nm in the supernatant (monitored by UV–Vis spectroscopy).

(EtOH) to 25-times (THF) higher than in water. In sum, the lipophilic CM can slowly pass the polar OS shell and is released from the nanocontainers with lipophilic conditions, so that insects are expected to be efficiently repelled if not killed. Based on the first synthesis and characterization of CM@OS core@shell nanocontainers, future biological studies are required to prove and to optimize the repellant and/or toxic effect on specific insects.

To evaluate the producibility of thin-films, 5 × 5 cm glass plates as substrates were cleaned with ethanol and water, followed by etching with hydrochloric acid. Subsequently, few drops of the nanocontainer suspension were doctor-bladed on these glass plates (Figure 8a). After slow solvent evaporation, transparent thin-films could be easily obtained (Figure 8b) and—according to SEM images—show a uniform dense coverage (Figure 8c). To demonstrate successful coating of the glass plates, we also used fluorescence-labeled CM/FR@OS nanocontainers that contain low quantities (0.01 mmol) of Fluorescence Red (FR) as an intensely emitting fluorescence dye. Due to the presence of FR, nanocontainers, suspensions and transparent thin-films show a weak red color (Figure 8d). Upon excitation with UV light

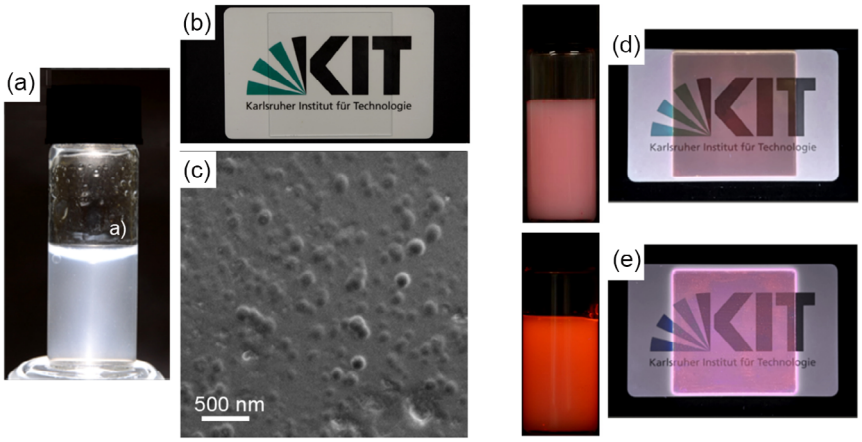

FIGURE 8 | Thin-film formation with CM@OS nanocontainers: (a) Photo of suspension in water in daylight; (b) doctor-bladed thin-film on glass plate in daylight; (c) SEM image of thin-film on glass plate shown in (b) after Pt-sputtering; (d) suspension (in water) and doctor-bladed thin-film of fluorescence-labeled CM/FR@OS nanocontainers (FR: fluorescence red) in daylight; and (e) suspension (in water) and doctor-bladed thin-film of fluorescence-labeled CM/FR@OS nanocontainers (FR: fluorescence red) under UV excitation (254 nm).

(254 nm), suspensions and transparent thin-films show intense red emission (Figure 8e). Both uniform red color of nonilluminated glass plates and emission of illuminated glass plates point to a uniform disposition of CM/FR@OS nanocontainers as thin-films.

3 | Conclusions

CM is a widely used insecticide, which, however, is also harmful to the environment. To this concern, nanocontainer systems can be suitable to reduce the required CM amount and the cycles of reapplication as well as to increase the photochemical stability of CM. CM@OS core@shell nanocontainers (OS: *n*-octylsilicate) are here presented as a novel material and concept. The CM@OS core@shell nanocontainers are synthesized via a solvent/antisolvent approach. They are characterized by a mean size of 34 ± 8 nm, a mean diameter of 15 ± 3 nm of the CM core, a mean OS shell thickness of 7 ± 2 nm, and a CM content of 10 wt%. Beside the general function as a nanocontainer wall to encapsulate CM, OS leads to a high negative surface charging (−63 ± 1 mV) due to the highly polar Si–O groups. As a result, the nanocontainers are colloidally very stable in aqueous suspensions. Moreover, OS allows a slow diffusion of the lipophilic CM through the OS shell due to the presence of the octyl functionality. The release of CM was exemplarily tested applying suspension media of different polarity, including water, ethanol and THF. Accordingly, the release rate can be directly correlated with the polarity of the respective solvent. The photochemical stability of the CM@OS core@shell nanocontainer was compared to free CM. Here, it turned out that the photostability—specifically the cleavage of the ester group and the cleavage of the cyclopropanyl ring of CM—is significantly slower after encapsulation in the nanocontainers. Finally, thin-films of CM@OS core@shell nanocontainers on glass plates were prepared, which, as expected, is straightforward for the nanocontainers due to the silica-based shell. Beside CM, synthesis and material concept of the core@shell nanocontainers can generally become suitable also for other insecticides or drugs.

4 | Experimental Section

4.1 | Chemicals

α-CM (98%, isomeric mixture, Thermo Fisher, Germany) or α-CM (p.a., Thermo Fisher, Germany); *n*-octyltriethoxysilane (95%, Thermo Fisher, Germany); ethanol (absolute, Merck, Germany); ammonium fluoride (≥98%, Merck, Germany); hydrochloric acid (37%, Merck, Germany); and ammonia (25%, Merck, Germany); Fluorescent Red (Kremer, Germany) were used as purchased.

4.2 | Synthesis of CM@OS Core–shell Nanocontainers

For the solvent/antisolvent synthesis of CM@OS core–shell nanocontainers, a solution of 20.0 mg of CM ($C_{22}H_{19}Cl_2NO_3$, 0.048 mmol) in 1.0 mL of *n*-octyltriethoxysilane (OTES, $C_{14}H_{52}O_3Si$, 0.88 g, 3.19 mmol) was prepared as the solvent solution. In addition, 2.0 mL of ethanol were added to the solvent solution to reduce its viscosity. The solvent solution was then injected into an antisolvent solution with 0.2 mL of 0.1 M HCl in 50 mL of demineralized water at 70°C with vigorous stirring. After 2 h of continuous stirring at 70°C, 1 mg of NH_4F was added as a flux to promote the formation of a silica network. After 6 h, 0.25 mL of aqueous ammonia (25%) were added, and after additional 24 h of continuous stirring at 70°C, the suspension was left to cool to room temperature. For purification, the suspension was centrifuged (8000 × g, 10 min) and the bottom phase removed. Due to the lower density of the CM@OS core@shell nanoparticles in comparison to water, they were located in the top phase, which was diluted with demineralized water. To remove remaining salts and starting materials, centrifugation and removal of bottom phase were repeated twice. Finally, the suspension of the CM@OS core@shell nanoparticles was stored at a concentration of up to 5 mg/mL. This suspension was colloidally stable for several weeks.

To obtain CM-free reference nanoparticles, the above recipe was performed without addition of CM. These CM-free reference nanoparticles were purified and handled as the above CM@OS core@shell nanoparticles.

If a fluorescence labeling of the CM@OS core@shell nanoparticles was required, 10 mg of red emitting dye Fluorescent Red (FR; 0.01 mmol) were added together with CM to the solvent solution.

The CM release was exemplarily tested with CM@OS core@shell nanocontainers, based on suspensions in water, ethanol and THF. To this concern, 100 mg of the nanocontainers were suspended in the respective solvent (5 mL) and stirred for 12 h. Thereafter, the nanocontainers were separated by centrifugation and the presence of CM in the supernatant analyzed via UV–Vis spectroscopy using the CM absorption at 276 nm.

4.3 | Analytical Equipment

DLS was performed to examine the hydrodynamic diameter of the CM@OS core@shell nanocontainers in suspension. To this concern, suspensions were analyzed in polystyrene cuvettes using a Nanosizer ZS (Malvern Instruments, United Kingdom). This device was also used for *zeta-potential analysis* to evaluate the pH-dependent surface charging and the colloidal stability the CM@OS core@shell nanocontainers.

SEM was used to determine the particle size, using a Zeiss Supra 40 VP (Zeiss, Germany). Samples were prepared by dappling small droplets of the CM@OS core@shell nanocontainer suspension in water on a silicon wafer, which was left to dry for at least 8 h at room temperature. At least 150 nanoparticles were statistically evaluated to determine mean particle diameter. The same device was also used for *scanning transmission electron microscopy* (*STEM*) to analyze particle size as well as the presence of the inner cavity and shell of the nanocontainers.

Transmission electron microscopy (*TEM*) and *HAAADF-STEM* were performed with a FEI Osiris ChemiSTEM microscope (FEI, Netherlands) at 200 kV. TEM samples were prepared by evaporating small droplets of aqueous nanocontainer suspensions on Lacey-film carbon copper TEM grids.

EDXS was applied to prove the presence of the core@shell structure and to obtain element mappings. To this concern, a Bruker Quantax system (XFlash detector, Bruker, Germany) was used, that was installed at the above FEI Osiris ChemiSTEM microscope.

FT-IR spectra were recorded with a Bruker Vertex 70 FT-IR spectrometer (Bruker, Germany). For this purpose, 300 mg of dried KBr were mixed with 1 mg of the CM@OS core@shell nanocontainers or 0.10 mg of the reference material, pestle, and thereafter pressed to pellets. These pellets were measured in transmission mode in the range of 4000–450 cm^{-1}.

For the determination of the photostability, suspensions of CM@OS core@shell nanocontainers in water (0.1 mg/mL) or solutions (2 mL) of pure CM in a 90:10 ethanol:water mixture (0.01 mg/mL) were irradiated with a UV lamp at 257 nm. After 0, 2, and 4 h, the respective sample was dried. The solid residue was mixed with 300 mg of KBr, pestled and pressed to pellets thereafter. These pellets were measured in transmission mode in the range of 4000–450 cm^{-1}.

EA (*C/H/N/S analysis*) of dried CM@OS core@shell nanocontainers was performed via thermal combustion with an Elementar Vario Microcube device (Elementar, Germany) at a temperature of about 1100°C.

UV–Vis spectra were recorded on a Shimadzu UV-2700 (Shimadzu, Japan), equipped with a deuterium discharge lamp (180–360 nm) and a quartz halogen lamp 360–800 nm).

For the determination of the photostability, UV–Vis spectroscopy was used to quantify the CM amount in the CM@OS core@shell nanocontainers according to the Kubelka–Munk formalism. The respective CM concentration was quantified by comparison with reference solutions with known CM concentration. CM@OS core@shell nanocontainer suspensions with 100 µg/mL were measured in quartz glass cuvettes (type Q, 170–2700 nm, spectral quality 6; Starna, Germany) with an integrating sphere in diffuse transmission geometry against the pure solvent as a reference. For solutions of freely dissolved CM in ethanol, a double-beam setup was used for transmission measurements with the corresponding pure solvent as a reference. The determination of the photostability were conducted with CM@OS core@shell nanocontainer suspensions in water (0.5 mg/mL) as well as solutions of pure CM in ethanol (0.05 mg/mL) as a reference. The CM reference needs to be dissolved in ethanol as CM is insoluble in water. Due to the fact that the formation of reactive oxygen species (ROS) under UV irradiation is much higher in water than in ethanol, the conditions are much more harsh for the CM@OS core@shell nanocontainers as for the reference. To study the photostability, nanocontainers and reference were irradiated with 220 nm UV light over 24 h. The absorption was monitored at 276 nm.

Photoluminescence (*PL*): Excitation and emission spectra of fluorescence-labeled CM@OS core@shell nanocontainers were recorded by using a Horiba Jobin Yvon Spex Fluorolog 3 spectrometer, equipped with a 450 W Xenon lamp, an integrating sphere (Ulbricht sphere) and a photomultiplier as detector.

Acknowledgments

The authors acknowledge Jens Treptow for performing TEM analysis. Furthermore, the authors thank BSc. Marvin L. Bojemüller for support within the Bachelor thesis.

Open Access funding enabled and organized by Projekt DEAL.

Conflicts of Interest

The authors declare no conflicts of interest.

Data Availability Statement

The data that support the findings of this study are available from the corresponding author upon reasonable request.

References

1. M. A. Beach, U. Nayanathara, Y. Gao, et al., "Polymeric Nanoparticles for Drug Delivery," *Chemical Reviews* 124 (2024): 5505–5616.

2. M. Manzano and M. Vallet-Regi, "Mesoporous Silica Nanoparticles for Drug Delivery," *Advanced Functional Materials* 30 (2020): 1902634.

3. M. Jones and R. L. Goodyear, "High-Throughput Purification in Drug Discovery: Scaling New Heights of Productivity," *ACS Medicinal Chemistry Letters* 14 (2023): 916–919.

4. V. V. Komnatnyy, T. E. Nielsen, and K. Qvortrup, "Bead-Based Screening in Chemical Biology and Drug Discovery," *Chemical Communications* 54 (2018): 6759–6771.

5. R. A. Gallego, M. P. Edwards, and T. P. Montgomery, "An Update on Lipophilic Efficiency as an Important Metric in Drug Design," *Expert Opinion on Drug Discovery* 19 (2024): 917–931.

6. Y. Seo, H. Lim, H. Park, et al., "Recent Progress of Lipid Nanoparticles-Based Lipophilic Drug Delivery: Focus on Surface Modifications," *Pharmaceutics* 15 (2023): 772.

7. S. Han, L. Mei, T. Quach, C. Porter, and N. Trevaskis, "Lipophilic Conjugates of Drugs: A Tool to Improve Drug Pharmacokinetic and Therapeutic Profiles," *Pharmaceutical Research* 38 (2021): 1497–1518.

8. A. K. Singh, M. N. Tiwari, O. Prakash, and M. P. Singh, "A Current Review of Cypermethrin-Induced Neurotoxicity and Nigrostriatal Dopaminergic Neurodegeneration," *Current Neuropharmacology* 10 (2012): 64–71.

9. D. J. Ecobichon, *Pesticides and Neurological Diseases* (CRC Press, 1993), 306, ISBN. 978-0-8493-4361-2.

10. H. Mehlhorn, *Encyclopedia of Parasitology*, 4th ed. (Springer, 2017).

11. S. Razzaque, M. Abubakar, M. A. Farid, et al., "Detection of Toxic Cypermethrin Pesticides in Drinking Water by Simple Graphitic Electrode Modified with Kraft lignin@Ni@gC_3N_4 nano-composite," *Journal of Materials Chemistry. B* 12 (2024): 9364–9374.

12. T. B. Pham, T. H. C. Hoang, V. C. Nguyen, D. C. Vu, H. Bui, and V. H. Pham, "Improved Versatile SERS Spheroid End-Facet Optical Fiber Substrate Based on Silver Nano-Dendrites Directly Planted with Gold Nanoparticles Using Dual-Laser Assisted for Pesticides Detection," *Optical Materials* 126 (2022): 112196.

13. P. A. Sundari and P. Manisankar, "Development of Nano Poly(3-Methyl Thiophene)/Multiwalled Carbon Nanotubes Sensor for the Efficient Detection of Some Pesticides," *Journal of the Brazilian Chemical Society* 22 (2011): 746–755.

14. S. Hussain, M. Ashafaq, S. Alshahrani, et al., "Cardioprotective Effects of Nano-Piperine Against Cypermethrin Toxicity Through Oxidative Stress, Histopathological and Immunohistochemical Studies in Male Wistar Rats," *Natural Product Communications* 18 (2023): 1934578X231154029.

15. S. Hussain, M. Ashafaq, S. Alshahrani, et al., "Hepatoprotective Effect of Curcumin Nano-Lipid Carrier against Cypermethrin Toxicity by Countering the Oxidative, Inflammatory, and Apoptotic Changes in Wistar Rats," *Molecules* 28 (2023): 881.

16. M. Ashafaq, S. Hussain, S. Alshahrani, et al., "Neuroprotective Effects of Nano-Curcumin against Cypermethrin Associated Oxidative Stress and Up-Regulation of Apoptotic and Inflammatory Gene Expression in Rat Brains," *Antioxidants* 12 (2023): 644.

17. P. Sow, S. Dey, R. Dey, et al., "Poly Lactide-Co-Glycolide Encapsulated Nano-Curcumin Promoting Antagonistic Interactions between HSP 90 and XRCC1 Proteins to Prevent Cypermethrin-Induced Toxicity: An in Silico Predicted In Vitro and In Vivo Approach," *Colloids Surfaces B* 220 (2022): 112905.

18. G. Bapat, J. Mulla, C. Labade, O. Ghuge, V. Tamhane, and S. Zinjarde, "Assessment of Recombinant Glutathione-S-Transferase (HaGST-8) Silica Nano-Conjugates for Effective Removal of Pesticides," *Environmental Research B*204 (2022): 112052.

19. Y. Xiang, G. Zhang, Y. Chi, D. Cai, and Z. Wu, "Fabrication of a Controllable Nanopesticide System with Magnetic Collectability," *Chemical Engineering Journal* 328 (2017): 320–330.

20. P. S. Karandikar, J. D. Rajput, S. D. Bagul, V. V. Gite, and R. S. Bendre, "Controlled Release Study of Phenol Formaldehyde Based Microcapsules Containing Various Loading Percentage of Core Cypermethrin at Different Agitation Rates," *Polymer Bull* 76 (2019): 2519–2536.

21. J. Feng, G. Yang, S. Zhang, Q. Liu, S. M. Jafari, and D. J. McClements, "Fabrication and Characterization of β-Cypermethrin-Loaded PLA Microcapsules Prepared by Emulsion-Solvent Evaporation: Loading and Release Properties," *Environmental Science and Pollution Research* 25 (2018): 13525–13535.

22. C.-M. Xia, Y.-F. Zhou, W.-Y. Nie, et al., "Fabrication and Characterization of Cypermethrin Nanocapsules in Miniemulsion Polymerization System," *Journal of Applied Polymer Science* 126 (2012): 1859–1866.

23. S. H. Bang, I. C. Hwang, Y. M. Yu, H. R. Kwon, D. H. Kim, and H. J. Park, "Influence of Chitosan Coating on the Liposomal Surface on Physicochemical Properties and the Release Profile of Nanocarrier Systems," *Journal of Microencapsulation* 28 (2011): 595–604.

24. W. Zou, Y. Zhao, Y. Deng, et al., "Preparation of Layered Beta-Cypermethrin-Carrying Microcapsules from Pickering Emulsion of Hollow Mesoporous Silica Nanoparticles," *Materials Today. Communications* 31 (2022): 103695.

25. S. Patela, J. Bajpaia, R. Sainia, A. K. Bajpaia, and S. A. Bose, "Sustained Release of Pesticide (Cypermethrin) from Nanocarriers: an Effective Technique for Environmental and Crop Protection," *Process Safety and Environmental Protection* 117 (2018): 315–325.

26. D. Rudolph, N. Redinger, K. Schwarz, et al., "Amorphous Drug Nanoparticles for Inhalation Therapy of Multidrug-Resistant Tuberculosis," *ACS Nano* 17 (2023): 9478–9486.

27. V. Rein, A. Meschkov, K. Hagens, et al., "Zirconyl Hydrogenphosphate Nanocontainers for Flexible Transport and Release of Lipophilic Cytostatics, Insecticides, and Antibiotics," *Advanced Functional Materials* 29 (2019): 1900543.

28. D. E. Bugarisand H.-C. zur Loye, "Materials Discovery by Flux Crystal Growth: Quaternary and Higher Order Oxides," *Angewandte Chemie International Edition* 51 (2012): 3780–3811.

29. G. A. Parks, "The Isoelectric Points of Solid Oxides, Solid Hydroxides, and Aqueous Hydroxo Complex Systems," *Chemical Reviews* 65 (1965): 177–198.

30. A. H. Jubert, M. L. Alegre, R. Pis Diez, A. B. Pomilio, and V. D.Szewczuk, "Vibrational Spectra, NMR and Theoretical Studies of the Enantiomers and Rotamers of Alpha-Cypermethrin," *Spectrochimica Acta. Part A: Molecular Spectroscopy* 66 (2007): 1208–1221.

31. D. A. Laskowski, "Reviews of Environmental Contamination and Toxicology," *Reviews of Environmental Contamination and Toxicology* 174 (2002): 49–170.

32. World Health Organization, *Environmental Health Criteria* 82 (1989): 33–39.

33. S. Pedersen, J. L. Herek, and A. H. Zewail, "The Validity of the "Diradical" Hypothesis: Direct Femtoscond Studies of the Transition-State Structures," *Science* 266 (1994): 1359–1364.

34. F. Gosetti, B. Bolfi, U. Chiuminatto, M. Manfredi, E. Robotti, and E. Marengo, "Photodegradation of the Pure and Formulated Alpha-Cypermethrin Insecticide Gives Different Products," *Environmental Chemistry Letters* 16 (2018): 581–590.

35. F. Jin, M. Wei, C. Liu, and Y. Ma, "The Mechanism for the Formation of OH Radicals in Condensed-Phase Water under Ultraviolet Irradiation," *PhysChemChemPhys* 19 (2017): 21453–21460.

36. D. Lin-Vien, N. B. Colthup, W. G. Fateley, and J. G. Grasselli, *The Handbook of Infrared and Raman Characteristic Frequencies of Organic Molecules* (Elsevier, 1991), 19–21.

37. Y. Nosaka and A. Y. Nosaka, "Generation and Detection of Reactive Oxygen Species in Photocatalysis," *Chemical Reviews* 117 (2017): 11302–11336.